Elucidate the Formation Mechanism of Particulate Nitrate Based on Direct Radical Observations in the Yangtze River Delta summer 2019

Tianyu Zhai[a], Keding Lu[a, b]*, Haichao Wang[c], Shengrong Lou[d], Xiaorui Chen[a,f], Renzhi Hu[e], Yuanhang Zhang[a, b]*

[a] State Key Joint Laboratory of Environmental Simulation and Pollution Control, College of Environmental Sciences and Engineering, Peking University, Beijing 100871, China.

[b] Collaborative Innovation Center of Atmospheric Environment and Equipment Technology, Nanjing University of Information Science & Technology, Nanjing 210044, China.

[c] School of Atmospheric Sciences, Sun Yat-sen University, Guangzhou 510275, China.

[d] State Environmental Protection Key Laboratory of Formation and Prevention of the Urban Air Complex, Shanghai Academy of Environmental Sciences, Shanghai, 200223, China.

[e] Key Laboratory of Environmental Optics and Technology, Anhui Institute of Optics and Fine Mechanics, Chinese Academy of Sciences, Hefei, 230031, China.

[f] Now at: Department of Civil and Environmental Engineering, The Hong Kong Polytechnic University, Hong Kong, China.

* Correspondence to:

Keding Lu (k.lu@pku.edu.cn), Yuanhang Zhang (yhzhang@pku.edu.cn)

Abstract. Particulate nitrate (NO_3^-) is ~~the~~ one of the dominant components of fine particles in China, especially during pollution episodes, and has a significant impact on human health, air quality, and climate. Here a comprehensive field campaign ~~which focus~~that focuses on the atmospheric oxidation capacity and aerosol formation, and their effects in the Yangtze River Delta (YRD) ~~had been~~was conducted from May to June, 2019 at a regional site in Changzhou, Jiangsu province in China. The concentration of NO_3^-, OH radical, N_2O_5, NO_2, O_3, and relevant parameters were measured simultaneously. We showed a high NO_3^- mass concentration with 10.6 $\pm$ 8.9 µg m^{-3} on average, which accounted for 38.3 % of total water-soluble particulate components and 32.0 % of total $PM_{2.5}$, ~~and~~ followed by the proportion of sulfate, ammonium, and chloride by 26.0 %, 18.0 ~~%~~%, and 2.0 %, respectively. This result confirmed that the heavy nitrate pollution in eastern China not only happened in winter but also ~~summer time. High~~in the summertime. This study's high nitrate oxidation ratio (NOR) ~~during this study~~ emphasizes the ~~strong~~solid atmospheric oxidation and fast nitrate formation capacity in YRD. It is found that OH + NO_2 ~~at~~during daytime dominates nitrate formation on clean days while N_2O_5 hydrolysis ~~largely~~vastly enhanced and ~~become~~became comparable with that of OH + NO_2 during polluted days (~~47.1~~67.2 % and ~~52.9 %).~~30.2 %, respectively). An updated observed-constrain Empirical Kinetic Modeling Approach (EKMA) was used to assess the kinetic controlling factors of both local O_3 and NO_3^- productions, which indicated that the O_3-targeted scheme (VOCs: NO_x = 2: 1) is ~~effective~~adequate to mitigate the O_3 and nitrate pollution coordinately during summertime in this region. Our results promote the understanding of nitrate pollution mechanisms and mitigation based on field observation and model simulation, and call for more ~~attentions~~attention to nitrate ~~pollutions~~pollution in the summertime.

Keywords:

Nitrate pollution; Dinitrogen pentoxide; Nitrate formation; Pollution mitigation

1 Introduction

Chemical compositions of fine ~~particle~~particles have been measured in China during ~~the~~ past twenty years, and secondary inorganic aerosol is regarded as one of the dominant species in aerosol (Cao et al., 2012; Hagler et al., 2006; Zhao et al., 2013; Andreae et al., 2008). Since the Air Pollution Prevention and Control Action Plan, there has been a significant decrease ~~of~~in SO_2, NO_2, and $PM_{2.5}$ concentration in China, while the inorganic nitrate ratio in $PM_{2.5}$ increased and became the considerable component in $PM_{2.5}$ (Shang et al., 2021; Zhang et al., 2022). Therefore, ~~the~~a comprehensive understanding of the particle nitrate ~~foramtion~~formation mechanism is essential and critical to ~~mitigate~~mitigating haze pollution in China.

~~A massive~~Massive research ~~have~~has been ~~taken~~done in China ~~for investigating~~to investigate nitrate formation ~~mechanism~~mechanisms, and a basic framework has been established (Sun et al., 2006; Chang et al., 2018; Wu et al., 2019). In the daytime, NO_2 + OH radical oxidation (Reaction 1) is the major particulate nitrate formation pathway. The product (HNO_3) reacts with alkaline ~~substance~~substances in aerosol ~~by which,~~ generating particulate nitrate. This pathway is mainly ~~controled~~controlled by ~~precurors~~precursors concentration as well as the gas-particle partition of gaseous nitric acid, and particulate nitrate depends on temperature, relative humidity (RH), NH_3 concentration, and aerosol acidity (Wang et al., 2009; Song and Carmichael, 2001; Meng et al., 2020; Zhang et al., 2021). At night, N_2O_5 uptake is ~~an important~~a vital nitrate formation pathway (Reaction 4)(Chen et al., 2020; Wang et al., 2022). N_2O_5 is formed through NO_2 + NO_3 (Reaction 3) and there ~~exsits~~exists a quick thermal equilibrium balance (K_{eq} = 5.5 × 10⁻¹⁷ cm⁻³ molecule⁻¹ s⁻¹, 298 K). However, ~~there are~~ two problems remain ambiguous in quantifying the contribution of N_2O_5 uptake to nitrate formation. The first is the N_2O_5 heterogeneous uptake ~~coefficent~~coefficient (γ) on ambient aerosol is highly varied with the range from 10⁻⁴ to 10⁻¹ based on previous lab and field ~~measurments~~measurements (Bertram and Thornton, 2009; Brown et al., 2009; Wang et al., 2017c; Wang and Lu, 2016). The other one is $ClNO_2$ production

yield which ~~inflences~~influences nitrate contribution ~~duo~~due to the ~~large~~extensive variation range (Phillips et al., 2016; Staudt et al., 2019; Tham et al., 2018). Both ~~the~~ two parameters are ~~hardly~~complex to well-predicted by current schemes. NO_2 heterogeneous uptake has been found nonnegligible for nitrate formation, which can be a vital pathway during heavy haze events, according to recent study (Qiu et al., 2019; Chan et al., 2021). The uptake coefficient and nitrate yield remain uncertain, as same as the N_2O_5 heterogeneous reaction. Besides, N_2O_5 homogeneous hydrolysis, ~~NO_2 heterogeneous uptake~~ and NO_3 radical oxidation have a minor contribution to particulate nitrate under ambient ~~condition (Brown et al., 2009; Seinfeld and Pandis, 2016).~~conditions(Brown et al., 2009; Seinfeld and Pandis, 2016).

$$NO_2 + OH \rightarrow HNO_3 \qquad \text{R1}$$

$$NO_2 + O_3 \rightarrow NO_3 + O_2 \qquad \text{R2}$$

$$NO_2 + NO_3 + M \rightarrow N_2O_5 + M \qquad \text{R3.1}$$

$$N_2O_5 + M \rightarrow NO_2 + NO_3 + M \qquad \text{R3.2}$$

$$N_2O_5 + (H_2O \text{ or } Cl^-) \rightarrow (2 - \varphi) NO_3^- + \varphi ClNO_2 \qquad \text{R4}$$
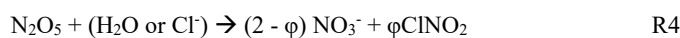
As a ~~key~~critical area of China's economy and industry, Yangtze River Delta (YRD) has suffered severe air pollution during past decades, and fine particle pollution in YRD has raised a widespread concern (Guo et al., 2014; Zhang et al., 2015; Zhang et al., 2017; Ming et al., 2017; Xue et al., 2019). However, most ~~of these~~ research ~~focus~~focuses on wintertime $PM_{2.5}$ pollution and ~~lack of~~lacks measurements of critical intermediate species and radicals to assess the importance of each nitrate formation pathway. In this study, with the direct measurements of hydroxyl radical and the reactive nitrogen compounds and chemical box model analysis, we explore the characteristics of nitrate and precursors in YRD in the summer of 2019, the importance of particulate nitrate formation pathways is quantified, and the ~~impact~~controlling factors are explored. ~~Further~~A further suggestion for summer pollution prevention and control ~~for~~in the local area is proposed.

2 Site description and methods

2.1 The campaign site

This campaign ~~had been taken~~took place at a ~~sub-urban~~suburban sanatorium from May 30th to June 18th, 2019 ~~at~~, in Changzhou, China. Changzhou (119.95 °E, 31.79 °N) is located ~~at~~in Jiangsu province and about 150 km northwest of Shanghai. The sanatorium ~~which is~~, located ~~at~~ 420 m east of Lake Ge (one of the largest lakes in Jiangsu province, 164 square kilometers~~)~~)), is surrounded by farmland and ~~fishpond~~fishponds. With the closest arterial traffic 1 km away, ~~there are~~ several industry zones are 4 km to the east. The prevailing wind was from the south and ~~south east~~southeast sectors (about 30 % of the time) compared to 20 % from the west sector, of which only 15 % came from the east. The wind speed was ~~normally~~usually lower than 5 m s^{-1} with faster speed from the west. This site was influenced by ~~both~~ anthropogenic and biological sources with ~~occasionally~~occasional biomass burning.
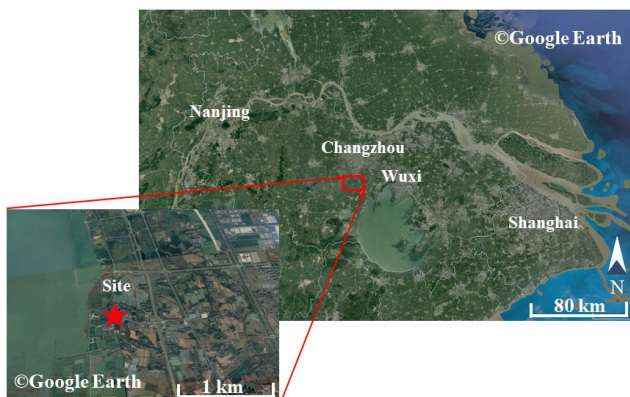
Figure 1 The location of the campaign site (red star), Changzhou, is ~~located~~ 150 km ~~at~~on the northwest side of Shanghai.

117 **2.2 The instrumentation**

118 ~~To comprehensive~~Multiple gaseous and particulate parameters were measured

119 simultaneously during the campaign to comprehensively interpret the nocturnal

120 atmospheric capacity and aerosol formation~~, multiple gas and particle parameters were~~

121 ~~measured simultaneously and the~~. The related instruments are listed in Table 1. N_2O_5

122 and Particle Number and Size Distribution (PNSD) were measured on the fourth floor

123 of the sanatorium, which is the top of the building. Other instruments were ~~set up~~placed

124 in containers ~~placed~~ on the ground ~~and~~ 170 m northeast of the building~~. These~~

125 ~~instruments monitored through the roof of containers and~~ and sampling inlets ~~were~~at

126 circa 5 m above the ground through the containers' roof.

127 N_2O_5 was measured by Cavity Enhanced Absorption Spectrometer (CEAS) based

128 on Lambert-Beer's law which was developed by (Wang et al., 2017b). Briefly, air

129 samples were drawn through the window and reached out of the wall 30 cm to prevent

130 influence from surface deposition. ~~Aerosol~~The aerosol membrane filter was deployed

131 before ~~sample~~the PFA sampling tube and changed every 2 hours ~~during the~~at night to

132 avoid a decrease in N_2O_5 transmission efficiency due to the increased loss of N_2O_5 from

133 the accumulated aerosols on the filter. N_2O_5 was decomposed to NO_3 and NO_2 through

134 preheating tube ~~which is~~heat at 130 °C and detected within a PFA-coated resonator

135 cavity ~~which is~~ heated at 110 °C to prevent the formation of N_2O_5 by reversible reaction

136 subsequently. At the end of each sampling cycle (5 min), a 30 s injection of high

137 concentration NO (10 ppm, 20 ml min^{-1}) ~~which~~ mixed with sample air was set to

138 eliminate NO_3-N_2O_5 in the system. The NO titration spectrums were adopted as the

139 dynamic background spectrum by assuming ~~that~~ no H_2O concentration variation in a

140 single sampling cycle. The loss of N_2O_5 in the sampling system and filter ~~were~~was also

141 considered ~~within~~during data correction. The limit of detection (LOD) was estimated

142 to be 2.7 pptv (1 σ) with an uncertainty of 19 %.

143 OH radical measurement was conducted by Fluorescence Assay by Gas Expansion

144 Laser-Induced Fluorescence techniques (FAGE-LIF~~), ambient~~). Ambient air was

145 expanded through a 0.4 mm nozzle to low pressure in a detection chamber, ~~in~~ where

146 ~~OH radical irradiated by~~ the 308 nm laser pulse irradiated OH radical at a repetition

147 rate of 8.5 kHz (Chen et al., 2018). NO_x and O_3 were monitored by commercial

148 monitors (Thermo-Fisher 42i and 49i). Volatile organic compounds (VOCs) were

149 measured by ~~using~~an automated Gas Chromatograph equipped with a Mass

150 Spectrometer and flame ionization detector (GC-MS) with a time resolution of 60 min.

151 The photolysis frequencies were determined from the spectral actinic photon flux

152 density measured by ~~spectroradiometer (Bohn et al., 2008)~~a spectroradiometer (Bohn

153 et al., 2008).

154     $PM_{2.5}$ concentration was obtained by Tapered Element Oscillating Microbalance

155 (TEOM 1405, Thermo Scientific Inc). Aerosol surface concentration (S_a) was

156 converted from particle number and size distribution, which was measured by Scanning

157 Mobility Particle Sizer (SMPS, TSI 3936) and Aerosol Particle Sizer (APS, TSI 3321)

158 and modified to the wet particle-state S_a with a hygroscopic growth factor (Liu et al.,

159 2013). The uncertainty of the wet S_a was ~ 30 %. Meanwhile, water-soluble particulate

160 ~~species as well as~~components and their gaseous precursors were analyzed through the

161 Monitor for AeRosols and GAses in ambient air (MARGA, Chen et al. (2017)).

162 Meteorological data were also available, including the temperature, relative humidity

163 (RH), pressure, wind speed, and wind direction~~, were also available~~.

164 **Table 1** The observed gas and particle parameters during the campaign.

Parameters	Detection of limit	Method	Accuracy
N_2O_5	2.7 pptv (1 σ, 1 min)	CEAS	± 19 %
OH	1.6×10^5 cm^{-3} (1 σ, 60 s)	LIF[a]	± 21 %
NO	60 pptv (2 σ, 1 min)	PC[c]	± 10 %
NO_2	0.3 ppbv (2 σ, 1 min)	PC[c]	± 10 %
O_3	0.5 ppbv (2 σ, 1 min)	UV photometry	± 5 %
VOCs	20-300 pptv (60 min)	GC-MS	± 15 %
$PM_{2.5}$	0.1 μg m^{-3} (1 min)	TEOM[d]	± 5 %
Photolysis frequencies	5×10^{-5} s^{-1} (1 min)	SR[e]	± 10 %
PNSD	14 nm -700 nm (4 min)	SMPS, APS	± 10 %
HNO_3, NO_3, HCl	0.06 ppbv (30 min)	MARGA[f]	± 20 %

| NH$_4^+$, NO$_3^-$, Cl$^-$, SO$_4^{2-}$ | 0.05 µg m^{-3} (30 min) | MARGA^f | ± 20 % |

165 ^{a} Laser-induced fluorescence; ^{b} Chemiluminescence; ^{c} Photolytic converter; ^{d} Tapered

166 Element Oscillating Microbalance; ^{e} Spectroradiometer; ^{f} the Monitor for AeRosols and

167 GAses in ambient air.

2.3 The empirical kinetic ~~modelling~~modeling approach

169 A box~~-~~ model coupled with the Regional Atmospheric Chemical Mechanism version 2

170 (RACM2, Goliff, Stockwell & Lawson, 2013) is used to conduct the mitigation

171 strategies studies. The model is operated in one-hour time resolution with measurement

172 results of temperature, relative humidity, pressure, CO, NO$_2$, H$_2$O, photolysis

173 frequencies, and aggregated VOCs input to constrain the model. It should be noted that

174 HONO concentration is ~~simply~~ calculated by NO$_2$ times 0.02 ~~which is,~~ as suggested by

175 Elshorbany et al. (2012), and has been used in the box model before (Lou et al., 2022).

176 Long-~~live~~lived species such as H$_2$ and CH$_4$ are ~~set~~assumed as constants (550 ppbv and

177 1900 ppbv, respectively). ~~What's more~~Moreover, a 13-hour constant loss rate of

178 unconstrained intermediate and secondary products, ~~which is~~ the result of synthetic

179 evaluating secondary simulation of secondary species, is set for representing the multi-

180 effects of deposition, transformation, and transportation.

181   The approaches ~~of~~to the chemical production of O$_3$ (P(O$_3$)) and inorganic nitrate

182 (P(NO$_3^-$)) are ~~using previously~~ described ~~expression~~in previous articles (Tan et al., 2021;

183 Tan et al., 2018) ~~in~~ and expressed as Equation 1 and 4:

$$P(O_3) = F(O_3) - D(O_3) \qquad \text{Eq1}$$

$$F(O_3) = k_{HO_2+NO}[NO][HO_2] + k_{(RO_2+NO)eff}[NO][RO_2] \qquad \text{Eq2}$$

$$D(O_3) = k_{OH+NO_2}[OH][NO_2] + (k_{OH+O_3}[OH] + k_{HO_2+O_3}[HO_2] + k_{alkenes+O_3}[alkenes])[O_3] \qquad \text{Eq3}$$

$$P(NO_3^-) = P(HNO_3) + P(pNO_3^-) \qquad \text{Eq4}$$

$$P(HNO_3) = k_{OH+NO_2}[OH][NO_2] \qquad \text{Eq5}$$

$$P(pNO_3^-) = 0.25(2 - \varphi) C \gamma S_a [N_2O_5] \qquad \text{Eq6}$$

184 briefly, P(O$_3$) is net ozone production, which is calculated by peroxyl radial + NO

185 oxidation (Eq. 2) minus the chemical loss of O$_3$ and NO$_2$ (Eq. 3). P(NO$_3^-$) is constituted

186 by reaction OH + NO$_2$ (Eq. 5) and N$_2$O$_5$ ~~heterogenous~~heterogeneous uptake (Eq. 6).

187 Here, rate constants of reactions are obtained from NASA JPL Publication ~~(Burkholder~~

188 ~~et al., 2015)~~ or RACM2 (Goliff et al., 2013). γ is the N$_2$O$_5$ uptake coefficient ~~which is~~

189 calculated from parameterization (γ$_P$, more details in chapter 3.3). φ represents ClNO$_2$

190 production yield through N_2O_5 hydrolysis, and the mean value reported ~~in~~by Xia et al.
191 (2020) ~~are~~is used in this work.

192 ~~Empirical~~The empirical Kinetic Modeling Approach (EKMA) was innovated ~~for~~
193 ~~studying~~to study the effects of precursors (VOCs~~,~~ and NO_x) reactivity on the
194 ~~region's~~region's ozone pollution by Kanaya et al~~.~~., which ~~help~~helps recognize the
195 region's susceptibility to precursors by weight and become a prevalent tool to study the
196 process of ozone formation (Tan et al., 2018; Yu et al., 2020b; Kanaya et al., 2008).
197 The prevention and control problem of pollutant generation can be transformed through
198 the EKMA curve to reduce its precursors' emissions. Furthermore, the
199 ~~precursors~~precursor reduction scheme needed for total pollutant ~~total~~ control is given
200 qualitatively. $P(NO_3^-)$ can also be analyzed through EKMA for the nonlinear secondary
201 formation relationship with precursor reactivity. Here, an isopleth diagram of the net
202 ozone production rate as functions of the reactivities of NO_x and VOCs can be derived
203 from EKMA. In detail, 0.01 to 1.2 emission reduction strategy assumptions are
204 exponential interpolation into 20 kinds of emission ~~situation~~situations of NO_x and
205 VOCs, respectively, which in total counts 400 scenarios.

2.4 The calculation of aerosol liquid water content

207 Aerosol liquid water content (ALWC) is calculated through ISORROPIA II
208 (Fountoukis and Nenes, 2007). Forward mode is applied in this study. Furthermore,
209 water-soluble ~~ions~~particulate components in $PM_{2.5}$ and gaseous species ($NH_3 + HNO_3 +$
210 HCl) obtained from MARGA, along with RH and T, are input as initial input. In
211 addition, metastable aerosol state is chosen ~~since~~due to high RH during this campaign.

3 Result and discussion

3.1 Overview of measurements

214 The time used in this study is China Standard Time (UTC + 8) and the local sunrise and
215 sunset time during the campaign were around 5 am and 7 pm, respectively. The whole
216 campaign period is divided into ~~the~~ four $PM_{2.5}$ clean periods and four $PM_{2.5}$ polluted
217 periods (9 out of 14 days, the latter polluted periods ~~and~~days day refer to $PM_{2.5}$ pollution

带格式的: 下标

218   except specified description) according to the Chinese National Air Quality Standard

219   (CNAAQS) Grade I of daily PM$_{2.5}$ concentrations (< 35.0 μg m^{-3}). Figure 2 shows the

220   meteorological parameters, and gas-phase and particulate species timeseries during the

221   observation. During the campaign, the temperature was high~~and~~; the maximum reached

222   34.5 ℃, with an average of 25.1 ± 3.7 ℃. RH changed drastically from 21 % to 88 %,

223   with a mean value ~~at~~of 58.9 ± 14.0 %. ~~Mean~~The mean NO$_2$ concentration was 14.8 ±

224   9.5 ppbv. Meanwhile, the O$_3$ average was 54.6 ± 28.8 ppbv, exceeding CNAAQS Grade

225   II for a maximum daily average of 8 h ozone (160 μg m^{-3}) on 14 out of 19 days and

226   exceeding 200 μg m^{-3} on ~~6~~six days.
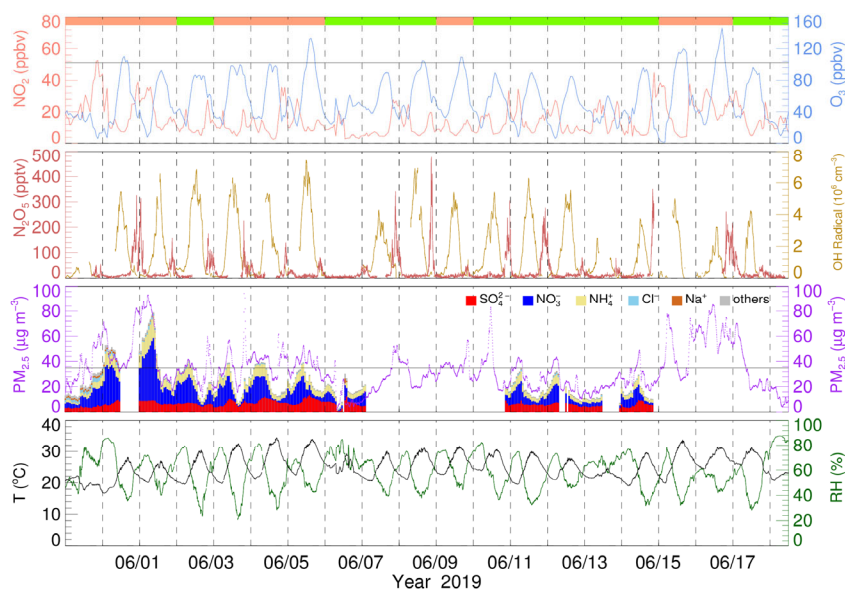
227
228   **Figure 2** Timeseries of NO$_2$, O$_3$, N$_2$O$_5$, OH radical, PM$_{2.5}$, and water-soluble particulate
229   ~~species~~components, temperature, and RH. The vertical dotted line represents the zero
230   clock. The black horizontal solid line in O$_3$ and PM$_{2.5}$ ~~panel~~panels represents Chinese
231   national air quality ~~standard~~standards for O$_3$ and PM$_{2.5}$, respectively. ~~Top~~The top panel
232   color blocks represent the PM$_{2.5}$ clean day (light green) and PM$_{2.5}$ polluted day(salmon~~)~~
233   ~~respectively.~~).

234

235   Daytime OH radical ranged from 2 × 10^6 to 8 × 10^6 molecular cm^{-3} with a daily

236   peak over 3 × 10^6 molecular cm^{-3}. Maximum OH radical reached 8.18 × 10^6 molecular

237 cm^{-3} in this campaign. ~~Comparing~~Compared with other summertime OH radical

238 observed ~~campaign~~ in China, OH radical concentration in this site is relatively low but

239 still on the same order of magnitude (Lu et al., 2012; Lu et al., 2013; Ma et al., 2022;

240 Tan et al., 2017; Woodward-Massey et al., 2020; Yang et al., 2021). N$_2$O$_5$ mean

241 concentration was 21.9 ± 39.8 pptv with a nocturnal average of 61.0 ± 63.1 pptv and a

242 daily maximum of over 200 pptv at ~~8~~eight nights. The maximum concentration of N$_2$O$_5$

243 (477.2 pptv, 5 min resolution) appeared at 20:47 on June 8th. The average NO$_3$ radical

244 production rate P(NO$_3$) is 2.1 ± 1.4 ppbv h^{-1} with nocturnal average P(NO$_3$) 2.8 ± 1.6

245 ppbv h^{-1} and daytime P(NO$_3$) 2.2 ± 1.4 ppbv h^{-1}. P(NO$_3$) is about twice of documented

246 value in Taizhou and North China Plain (Wang et al., 2017a; Wang et al., 2018b; Wang

247 et al., 2020a), but close to another result in YRD before (Chen et al., 2019). ~~Average~~

248 ~~of~~The average PM$_{2.5}$ was 34.6 ± 17.8 μg m^{-3} with a maximum reach of 163.0 μg m^{-3}.

249 The water-soluble particulate components of PM$_{2.5}$ are displayed as well~~, the~~. The

250 average NO$_3^-$ concentration was 10.6 μg m^{-3}, which accounts for 38.3 % mass

251 concentration of water-soluble particulate components and 32.0 % total PM$_{2.5}$, while

252 the proportion of sulfate, ammonium, and chloride ~~are~~is 26.0 %, 18 ~~%~~%, and 2.0 %

253 respectively. To sum up, during the campaign period, the pollution of PM$_{2.5}$ would be

254 generally exacerbated ~~in general~~ on high O$_3$ and NO$_2$ days. Precipitation occurred

255 during four clean processes receded pollutant concentration~~,~~; otherwise, the pollution

256 condition remained severe.

257 The mean diurnal variations (MDC) of temperature, RH, NO$_2$, O$_3$, P(NO$_3$), N$_2$O$_5$,

258 OH radical, and PM$_{2.5}$ in different air quality are shown in Figure 3. The temperature,

259 RH, and OH radical MDC show indistinctive ~~difference~~differences between clean

260 ~~day~~days (CD) and polluted ~~day~~days (PD). The MDC of NO$_2$ has two concentration

261 peaks ~~appeal~~that appear at 06:00 and 21:00 on CD, while at PD, its peak ~~appeals~~appears

262 at 20:00 and ~~maintain~~maintains a high level during the whole night. O$_3$ diurnal pattern

263 reflects a typical urban-influenced character with a maximum O$_3$ peak that lasts four

264 hours from 14:00 to 17:00 ~~with~~, while polluted-day O$_3$ peak concentration is 1.2 higher

265 than clean-day. P(NO$_3$) grows after the O$_3$ peak and maximum P(NO$_3$) shows at 19:00

266 with an average value of 1.7 ppbv h^{-1} on ~~clean day~~CD. By contrast, the mean polluted-

267 day P(NO3) is 2.6 ppbv h-1, and the maximum value ~~reach~~reaches 4.7 ppbv h^{-1}. In

268 contrast, the clean-day N$_2$O$_5$ has a higher average and maximum concentration than PD,

269 which suggests a faster removal process during PD. PM$_{2.5}$ ~~have~~has a similar trend with

270 P(NO$_3$) and has a higher concentration during nighttime.

271
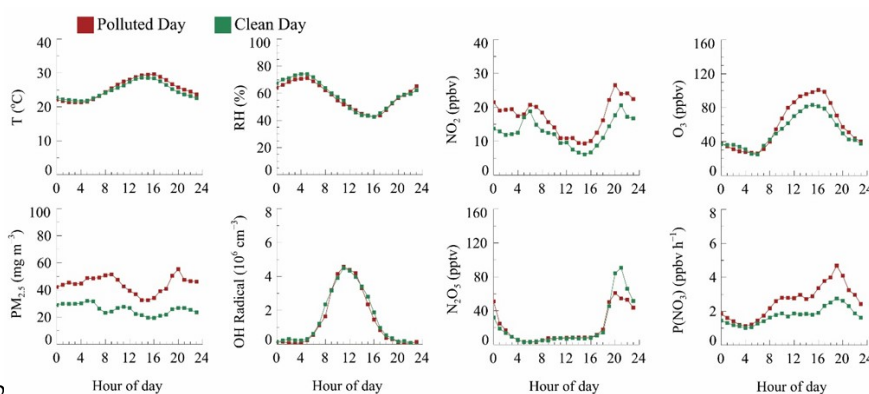
273 **Figure 3** The mean diurnal variations of temperature, RH, NO$_2$ (Salmon), O$_3$, P(NO$_3$),

274 N$_2$O$_5$, OH radical(orange~~)~~), and PM$_{2.5}$ of clean day and polluted day.

275 **3.2 The evolution of nitrate pollution**

276 Figure 4 (a) shows the relationship ~~of~~between nitrate and sulfate with water-soluble

277 ~~ion.~~particulate components. Nitrate ~~has positive correlation~~positively correlates with

278 ~~particulate~~total water-soluble ~~ion~~particulate components, while the sulfate ratio

279 ~~having~~has an inverse correlation. With PM$_{2.5}$ concentration increasing, nitrate

280 proportion ~~increasing~~increases rapidly and ~~keep~~keeps high weight at heavy PM$_{2.5}$

281 period while sulfate ~~appears~~ratio pears opposite phenomenon. Once the mass

282 concentration of total water-soluble ~~ion~~particulate component is over 30 μg m^{-3}, the

283 mass fraction of nitrate in total water-soluble ~~ion~~particulate components is up to 50 %

284 on average. This result illustrates that particulate nitrate is one of the vital sources of

285 explosive growth particulate matter explosive growth.
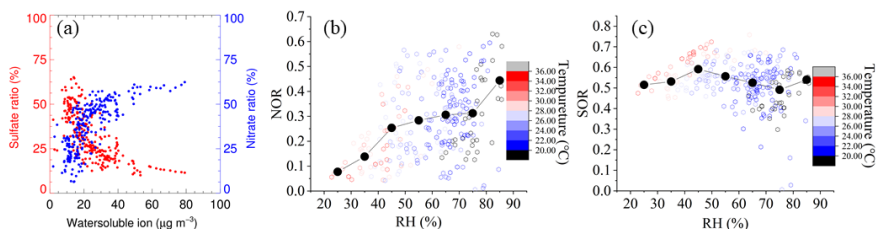
286
287 **Figure 4** (a) Particulate ion mass concentration ratio of nitrate and sulfate to water
288 soluble ion. (b) NOR against RH, colored with temperature. (c) SOR against RH,
289 colored with temperature.

290

291 To further assess the conversion capacity of nitrate and sulfate in this site, the sulfur
292 oxidation ratio (SOR) and the nitrogen oxidation ratio (NOR) are used ~~for indicating~~to
293 indicate the secondary transformation ratio of SO_2 and NO_2, respectively ~~(Sun et al.,~~
294 ~~2006).~~(Sun et al., 2006). SOR and NOR are estimated using the formulae below:

295

$$SOR = \frac{nSO_4^{2-}}{nSO_4^{2-}+nSO_2} \qquad Eq7$$

$$NOR = \frac{nNO_3^-}{nNO_3^-+nNO_2} \qquad Eq8$$

296 ~~here~~Where n refers to the molar concentration~~. The~~, the higher SOR and NOR represent
297 more oxidation of gaseous species into a secondary aerosol. As depicted in Figure 4 (b-
298 c), NOR ~~rapid~~rapidly increases at RH < 45 %, remains constant at 45 % < RH < 75 ~~%~~%,
299 and ends with a ~~sharply~~sharp increase at RH > 75 %. ~~In addition, NOR has inverse~~
300 ~~correlation with temperature which reflects the importance of nighttime secondary~~
301 ~~transformation and the influence of negative correlation of gas-solid equilibrium~~
302 ~~between particulate nitrate and gaseous HNO₃.~~ During the study period, not only is the
303 average concentration of NO2 ~~is~~ higher among PD~~,~~ but ~~also~~ there is ~~significate~~also a
304 significant difference between PD and CD NOR. The average values of NOR are 0.32
305 in PD~~,~~ and 0.25 in CD~~,~~ respectively~~,~~ which manifests ~~that~~ the more secondary

306 transformation and pollution potential in PD. ~~On the~~In contrast, the SOR stays constant

307 at a high value (~ 0.5) during the whole RH scale, which shows a different pattern ~~with~~

308 ~~previously~~from previous research (Li et al., 2017; Zheng et al., 2015). One possible

309 explanation is that SO$_2$ concentration stays low ~~level~~ during the whole campaign (4.4 ±

310 2.4 ppbv on average~~)~~), and SO$_2$ oxidation depends on the limit of SO$_2$ instead of

311 oxidation capability. Meanwhile, the mean SOR in both situations ~~are~~is over 0.5 (0.52

312 in CD and 0.56 in PD), further supporting the SO$_2$ limited hypothesis. Besides, Table 2

313 ~~summaries~~summarizes NOR and SOR values in YRD. NOR and SOR in this study are

314 similar ~~with~~to values reported in other YRD research (Shu et al., 2019; Zhang et al.,

315 2020b; Qin et al., 2021; Zhao et al., 2022), except values in 2013 ~~(Wang et al., 2016)~~,

316 but higher than north China study ~~(Cao et al., 2017)~~ which emphasize the ~~strong~~solid

317 atmospheric oxidation capacity in YRD region.

Table 2 Statistical result of NOR and SOR in YRD

Location and Year	SOR				NOR				References
	Max	Min	Mean	SD	Max	Min	Mean	SD	
Nanjing 2013 Winter	0.42	0.10	0.28	0.11	0.29	0.15	0.21	0.05	
Suzhou 2013 Winter	0.41	0.15	0.27	0.11	0.30	0.06	0.16	0.08	
Lin'an 2013 Winter	0.50	0.19	0.35	0.11	0.24–	0.12	0.18	0.05	
~~Hanghou~~Hangzhou 2013 Winter	0.30–	0.14	0.21	0.06	0.11–	0.06	0.09	0.02	~~(Wang et al., 2016)~~
Ningbo 2013 Winter	0.35–	0.09	0.21	0.11	0.23–	0.03	0.11	0.07	
YRD 2016 Summer	-	-	0.347	-	-	-	0.11	-	~~(Shu et al., 2019)~~
YRD 2016 Winter	-	-	0.247	-	-	-	0.15	-	
Nanjing 2019 spring	0.48	0.38	-	-	0.31	0.29	-	-	~~(Qin et al., 2021)~~
Changzhou 2019 spring	0.35	0.3	-	-	0.27	0.23	-	-	
Changzhou 2019 Winter	0.68	0.24	0.35	0.12	0.44	0.13	0.2	0.1	~~(Zhang et al., 2020b)~~
Changzhou 2019 Summer	0.16	0.76	0.54	0.1	0.08	0.63	0.28	0.14	This work

319 **3.3 The derivation of N$_2$O$_5$ uptake coefficient**

320 Statistical analysis of the observation above highlights the ~~fast~~rapid formation of

321 particulate nitrate. ~~In order to~~To assess the contribution of N$_2$O$_5$ hydrolysis to particular

322 nitrate formation, two methods are applied to calculate the N$_2$O$_5$ uptake coefficient. The

323 first method is a stationary-state approximation (Brown et al., 2003). By assuming that

324 the rates of production and loss of N_2O_5 are approximately in balance, the total loss rate

325 of N_2O_5 ($k_{N_2O_5}$) can be calculated through equation 9. The $k_{N_2O_5}$ is main dominated by

326 N_2O_5 heterogeneous uptake, since homogeneous hydrolysis of N_2O_5 ~~contributes very~~

327 ~~little~~contribute tiny (Brown and Stutz, 2012). N_2O_5 uptake coefficient through steady-

328 state (note as γ_S) is derived as equation 10. Here C is the mean molecule speed of N_2O_5,

329 and S_a is the aerosol surface concentration.

$$\tau_{ss}(N_2O_5) = \frac{[N_2O_5]}{k_{R3.1}[NO_2][O_3]} = (k_{N_2O_5} + \frac{k_{NO_3}}{K_{eq}[NO_2]})^{-1} \qquad \text{Eq9}$$

$$k_{N_2O_5} = 0.25 \, C \, \gamma_S \, S_a \qquad \text{Eq10}$$

330 Due to the fast variety of NO_3 loss ~~rate~~rates from VOCs, the steady-state method has

331 been unattainable in conditions affected by emission interferences. During the whole

332 campaign, we only retrieve three valid fitting results. As shown in Figure 5, the fitted

333 γ_S ~~are~~ranged from 0.057 to 0.123, which ~~are~~is comparable with Taizhou (0.041, Wang

334 et al. (2020a)) and much higher than other results in China (Yu et al., 2020a; Wang et

335 al., 2018a; Wang et al., 2020b; Wang et al., 2017a). The calculated k_{NO_3} ranged from

336 0.002 to 0.16 s^{-1}, represents drastic VOCs change during this campaign.
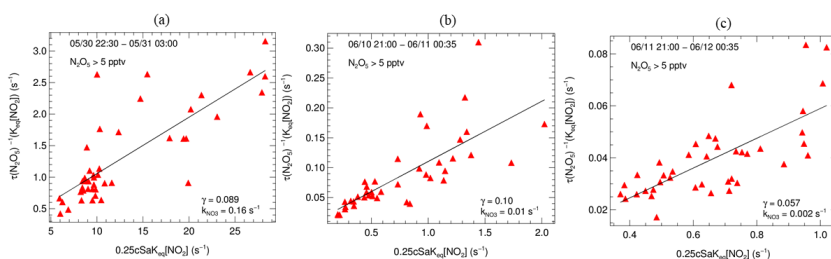
337

338 **Figure 5** Derived N_2O_5 uptake coefficients from N_2O_5 steady lifetime (γ~~($N_2O_5\_S$)~~_S)

339 with NO_2 and S_a, plots (a-c) represent the linear fitting results ~~at~~on the nights of 05/30,

340 06/10, and 06/11, respectively.

341   The other approach is the parameterization by (Yu et al., 2020a) which is depicted

342 as follows:

$$\gamma_{\_P} = \frac{4}{c}\frac{V_a}{S_a}\, K_H \times 3.0 \times 10^4 \times [H_2O] \left(1 - \frac{1}{\left(0.033 \times \frac{[H_2O]}{[NO_3^-]}\right)+1+\left(3.4 \times \frac{[Cl^-]}{[NO_3^-]}\right)}\right) \qquad Eq11$$

~~where~~Where V_a/S_a is the measured aerosol volume to surface area ratio by SMPS; K_H is ~~Henry's~~Henry's law coefficient which is set as 51 as recommended; $[NO_3^-]$ and $[Cl^-]$ are aerosol inorganic concentration measured by Marga; $[H_2O]$ is aerosol water content calculated through ISORROPIA II. ~~The parameterization calculated N_2O_5 uptake coefficient (note as $\gamma_{\_P}$) vary from 0.014 to 0.094 with average 0.035~~The valid parameterization calculated N_2O_5 uptake coefficient (note as $\gamma_{\_P}$) from May 30th to June 08th, 2019, shows in Figure 6 a good consistency between the trends of $\gamma_{\_P}$ and aerosol water content. Nighttime $\gamma_{\_P}$ varies from 0.001 to 0.024 with an average of 0.069 ± 0.0050 in polluted condition and 0.0036 ± 0.0026 in clean condition. The N_2O_5 uptake coefficient shows a good correlation between RH and aerosol water content. For the N_2O_5 uptake coefficient, although particulate nitrate mass concentration increased during the pollution event, an antagonistic effect on the N_2O_5 uptake coefficient was not obvious for the nitrate molarity decreasing.

Furthermore, we compare the difference between $\gamma_{\_S}$ and $\gamma_{\_P}$. Taking the night of May 30th as ~~an~~ example, the $\gamma_{\_S}$ is 0.~~100~~089 while $\gamma_{\_P}$ ranges from 0.~~021~~024 to 0.~~037~~057 with ~~an~~ average value ~~as~~of 0.~~026~~013 ± 0.0051. The difference between steady-state and parameterization is significant~~.~~; one possible explanation is uncertainty for stationary-state approximation caused by local NO or VOCs emission (Brown et al., 2009; Chen et al., 2022). Another reason is that parameterization by Yu et al. ignores the impact of organic matter on the fine particle. The difference in aerosol composition between this work and Yu et al may also bring uncertainty. Overall consideration, $\gamma_{\_P}$ will be chosen for the N_2O_5 heterogeneous uptake coefficient in later analysis and discussion.
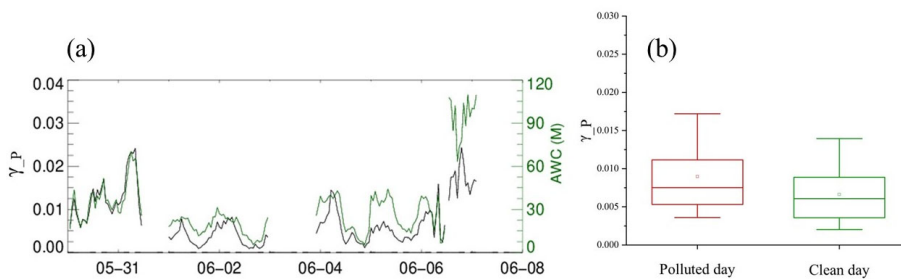
367

368 **Figure 6** Results of N$_2$O$_5$ uptake coefficients through parameterization (γ $_p$). (a) shows
369 timeseries of γ $_p$ and ISORROPIA II results of aerosol water content (AWC). (b) is the
370 box-plot of γ $_p$ on the polluted day and clean day, the hollow square represents the mean
371 value, and the solid line across the box shows the median score for the data set, while
372 the top and bottom whiskers represent 90 % and 10 % value of γ $_p$, respectively.

373 **3.4 Quantifying the contribution of nitrate formation pathways**

374 After the N$_2$O$_5$ uptake coefficient is counted, nitrate production potential (P(NO$_3^-$)) can
375 be calculated. Here N$_2$O$_5$ uptake coefficient is set as 0.~~035~~036 on clean day and 0.069
376 on polluted day, respectively, which ~~is~~are the average value derived from
377 parameterization~~, while the~~. The production ratio of NO$_3^-$ (by considering ClNO$_2$ yield
378 of 0.54) is set as 1.46 ~~from~~in the former study (Xia et al., 2020). Gas particle distribution
379 is considered by the result of particular nitrate and gas-phase nitrate by MARGA (input
380 HNO$_3$/NO$_3^-$ ratio to the model as OH + NO$_2$ nitrate production rate). ~~Subsequent~~
381 ~~discussion focuses on OH + NO$_2$ and N$_2$O$_5$ heterogeneous uptake~~NO$_2$ heterogeneous
382 uptake coefficient is set as 5.8 × 10^{-6} depending on the report by Yu et al. (2021) which
383 is the result of 70% RH on urban grime.

384   The mean diurnal variations of the nitrate production potential of clean and polluted
385 day are depicted in Figure ~~6~~7. The OH + NO$_2$ pathway shows no significate difference
386 between clean and polluted day and ~~dominate~~dominates clean day nitrate formation
387 potential. Since the level of OH and NO$_2$ is less affected by the fine particle level.
388 However, the rapid increase of the N$_2$O$_5$ heterogeneous uptake pathway on polluted day
389 is fatal, and its peak formation rate at night over the OH + NO$_2$ pathway ~~which~~ can be

0390 used to explain nighttime nitrate explosive growth.

391 As shown ~~as~~in Figure ~~6c~~7c, OH + NO_2 ~~dominate~~dominates nitrate production on

392 clean day, while the N_2O_5 uptake pathway only contributes 13.~~2~~6 μg m^{-3}. On polluted

393 days, the ability of N_2O_5 uptake ~~grow~~grows fast ~~which reached 25.3~~, reaching 50.1 μg

394 m-3, while the OH pathway ~~don't~~doesn't change ~~too~~ much. There is no distinct

395 difference ~~of~~in the daytime pathway (OH + NO_2) between clean day and polluted day,

396 while the nighttime pathway ratio rises from 38.~~4~~1 % on clean day to ~~52.9~~67.2 % on

397 polluted day. ~~The~~NO_2 heterogeneous uptake increases from 0.93 μg m^{-3} on clean day to

398 2.0 μg m^{-3} on polluted day, but the contribution proportion does not change obviously.

399 Both the higher N_2O_5 uptake coefficient and higher S_a on polluted day increase the

400 contribution of N_2O_5 hydrolysis on particular nitrate ~~is vital~~ at pollution condition.

401
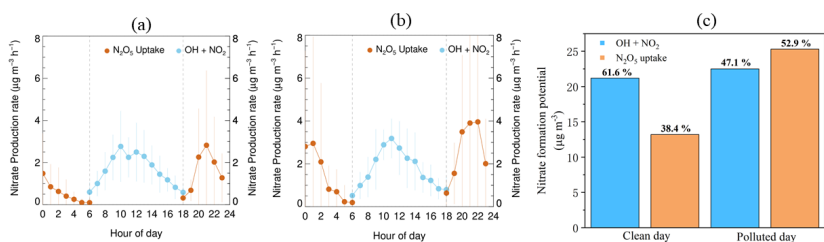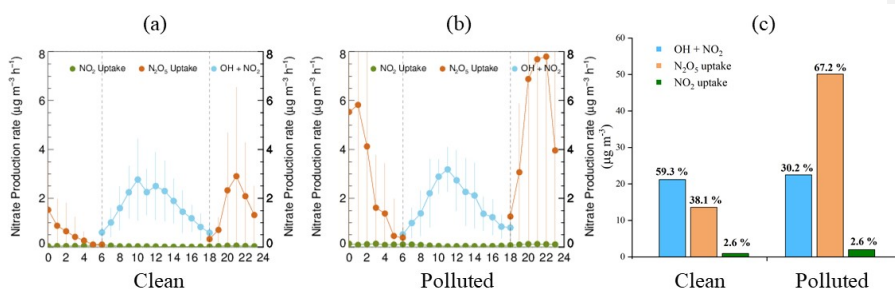
404 **Figure** ~~6~~7 The mean diurnal variations of the nitrate production potential of clean day(a)
405 and polluted day (b) and the $P(NO_3^-)$ distribution of clean and polluted day (c).

3.5 Mitigation strategies of particulate nitrate and ozone productions

407 We selected two pollution episodes (Episode I (2019.05.30 00:00 - 2019.06.02 00:00)

00018

408 and IV (2019.06.14 17:30 - 2019.06.17 12:00)) to explore the mitigation way of ozone

409 and nitrate pollution. Figure 78 shows the EKMA of $P(O_3)$ and $P(NO_3^-)$ of these two

410 periods, O_3 located at VOCs controlling area in the two pollution episodes, which

411 consist with previous YRD urban ozone sensitivity study (Jiang et al., 2018; Zhang et

412 al., 2020a; Xu et al., 2021). The best precursor reduction for O_3 is VOCs: NO_x = 2:1

413 while nitrate is located at the transition area, which means either of the precursors

414 reduction will mitigate nitrate pollution. For the regional and complex air pollution

415 characteristics in this region, a fine particle-targeting reduction scheme will aggravate

416 O_3 pollution. In contrast, the O_3-targeting scheme can mitigate O_3 and fine particle

417 simultaneously.

Polluted episode I

Polluted episode IV
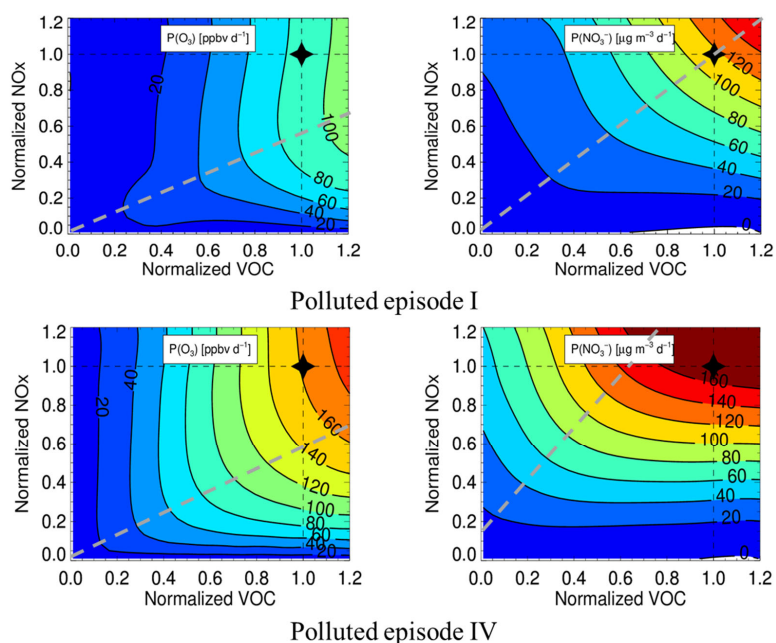
418

419 **Figure 78** Isogram of $P(O_3)$ and $P(NO_3^-)$ of polluted episode I (2019.05.30 00:00 -
420 2019.06.02 00:00) and IV (2019.06.14 17:30 - 2019.06.17 12:00) with different NOx
421 and VOC reduction degree. GreyThe grey dash line represents the ridge line.

422 **4 Conclusion**

423 A comprehensive campaign was conducted to interpret the atmospheric oxidation

424 capacity and aerosol formation duringfrom May 30th to June 18th18th, 2019 at, in

Changzhou, China. The high O_3 and $PM_{2.5}$ ~~concentration~~concentrations confirm complex air pollution characteristics in Changzhou~~,~~. and nitrate accounts for 38.3 % mass concentration of total water-soluble particulate components and 32.0 % of total $PM_{2.5}$. In addition, the average values of NOR are 0.32 in PD~~,~~ and 0.25 in CD. The positive correlation between NOR and RH and inverse correlation refer to the contribution of N_2O_5 ~~heterogenous~~heterogeneous uptake to nitrate formation.

Based on field observations of OH and related parameters, we show OH oxidation of the NO_2 pathway steadily ~~contribute~~contributes to nitrate formation no matter the clean or polluted period and domination clean day nitrate production (about 22 $\mu g\ m^{-3}$). N_2O_5 heterogeneous uptake contribution ~~grow rapidly~~proliferated on polluted day, from 13.~~2~~6 $\mu g\ m^{-3}$ (38.~~4 %) in~~1 %) on clean days to ~~25.3~~50.1 $\mu g\ m^{-3}$ (~~52.9 %) in~~67.2 %) on polluted days. NO_2 heterogeneous uptake contributes minor to nitrate formation (2.6 %).

The precursor reduction simulation suggests the reduction ratio of VOCs: NO_x equals 2:1 can simultaneously and effectively mitigate O_3 and fine particle pollution during the summertime complex pollution period in Changzhou. ~~In order to~~To more precisely and delicately establish a cooperative control scheme for regional O_3 and nitrate, the regional and long-time ~~filed~~field campaigns are needed in the future~~,~~ to analyze the seasonal and interannual variation of O_3 and nitrate and relevant parameters.

Code/Data availability. The datasets used in this study are available from the corresponding author upon request (k.lu@pku.edu.cn).

Author contributions. K.D.L. and Y.H.Z. designed the study. T.Y.Z analyzed the data and wrote the paper with input from all authors.

Competing interests. The authors declare that they have no conflicts of interest.

Acknowledgments. This project is supported by the National Natural Science Foundation of China (21976006); the Beijing Municipal Natural Science Foundation for Distinguished Young Scholars (JQ19031); the National Research Program for Key Issue in Air Pollution Control (DQGG0103-01, 2019YFC0214800). Thanks for the data

456   contributed by field campaign team.

457 **References**

458 Andreae, M. O., Schmid, O., Yang, H., Chand, D., Yu, J. Z., Zeng, L.-M., and Zhang,
459   Y.-H.: Optical properties and chemical composition of the atmospheric aerosol in
460   urban Guangzhou, China, Atmospheric Environment, 42, 6335-6350,
461   10.1016/j.atmosenv.2008.01.030, 2008.
462 Bertram, T. H. and Thornton, J. A.: Toward a general parameterization of N2O5
463   reactivity on aqueous particles: the competing effects of particle liquid water,
464   nitrate and chloride, Atmospheric Chemistry and Physics, 9, 8351-8363,
465   10.5194/acp-9-8351-2009, 2009.
466 Bohn, B., Corlett, G. K., Gillmann, M., Sanghavi, S., Stange, G., Tensing, E.,
467   Vrekoussis, M., Bloss, W. J., Clapp, L. J., Kortner, M., Dorn, H. P., Monks, P.
468   S., Platt, U., Plass-Dülmer, C., Mihalopoulos, N., Heard, D. E., Clemitshaw, K.
469   C., Meixner, F. X., Prevot, A. S. H., and Schmitt, R.: Photolysis frequency
470   measurement techniques: results of a comparison within the ACCENT project,
471   ACP, 8, 5373-5391, 10.5194/acp-8-5373-2008, 2008.
472 Brown, S. S. and Stutz, J.: Nighttime radical observations and chemistry, Chemical
473   Society Reviews, 41, 6405-6447, 10.1039/c2cs35181a, 2012.
474 Brown, S. S., Stark, H., and Ravishankara, A. R.: Applicability of the steady state
475   approximation to the interpretation of atmospheric observations of NO3 and
476   N2O5, Journal of Geophysical Research-Atmospheres, 108, 10,
477   10.1029/2003jd003407, 2003.
478 Brown, S. S., Dube, W. P., Fuchs, H., Ryerson, T. B., Wollny, A. G., Brock, C. A.,
479   Bahreini, R., Middlebrook, A. M., Neuman, J. A., Atlas, E., Roberts, J. M.,
480   Osthoff, H. D., Trainer, M., Fehsenfeld, F. C., and Ravishankara, A. R.: Reactive
481   uptake coefficients for N2O5 determined from aircraft measurements during the
482   Second Texas Air Quality Study: Comparison to current model
483   parameterizations, Journal of Geophysical Research-Atmospheres, 114,
484   10.1029/2008jd011679, 2009.
485 Burkholder, J. B., Sander, S. P., Abbatt, J., Barker, J., Huie, R., Kolb, C. E., Kurylo,
486   M., Orkin, V., Wilmouth, D. M., and Wine, P.: Chemical Kinetics and
487   Photochemical Data for Use in Atmospheric Studies, Evaluation Number 18,
488   10.13140/RG.2.1.2504.2806, 2015.
489 Cao, J.-J., Shen, Z.-X., Chow, J. C., Watson, J. G., Lee, S.-C., Tie, X.-X., Ho, K.-F.,
490   Wang, G.-H., and Han, Y.-M.: Winter and Summer PM2.5 Chemical
491   Compositions in Fourteen Chinese Cities, J Air Waste Manage, 62, 1214-1226,
492   10.1080/10962247.2012.701193, 2012.
493 Cao, Z., Zhou, X., Ma, Y., Wang, L., Wu, R., Chen, B., and Wang, W.: The
494   Concentrations, Formations, Relationships and Modeling of Sulfate, Nitrate and
495   Ammonium (SNA) Aerosols over China, Aerosol and Air Quality Research, 17,

496   84-97, 10.4209/aaqr.2016.01.0020, 2017.

497   Chan, Y. C., Evans, M. J., He, P. Z., Holmes, C. D., Jaegle, L., Kasibhatla, P., Liu, X.
498   Y., Sherwen, T., Thornton, J. A., Wang, X., Xie, Z. Q., Zhai, S. T., and
499   Alexander, B.: Heterogeneous Nitrate Production Mechanisms in Intense Haze
500   Events in the North China Plain, Journal of Geophysical Research-Atmospheres,
501   126, 10.1029/2021jd034688, 2021.

502   Chang, Y. H., Zhang, Y. L., Tian, C. G., Zhang, S. C., Ma, X. Y., Cao, F., Liu, X. Y.,
503   Zhang, W. Q., Kuhn, T., and Lehmann, M. F.: Nitrogen isotope fractionation
504   during gas-to-particle conversion of NOx to NO3- in the atmosphere -
505   implications for isotope-based NOx source apportionment, Atmospheric
506   Chemistry and Physics, 18, 11647-11661, 10.5194/acp-18-11647-2018, 2018.

507   Chen, H., Hu, R., Xie, P., Xing, X., Ling, L., Li, Z., Wang, F., Wang, Y., Liu, J., and
508   Liu, W.: A hydroxyl radical detection system using gas expansion and fast gating
509   laser-induced fluorescence techniques, J. Environ. Sci., 65, 190-200,
510   10.1016/j.jes.2017.03.012, 2018.

511   Chen, X., Walker, J. T., and Geron, C.: Chromatography related performance of the
512   Monitor for AeRosols and GAses in ambient air (MARGA): laboratory and
513   field-based evaluation, Atmos. Meas. Tech., 10, 3893-3908, 10.5194/amt-10-
514   3893-2017, 2017.

515   Chen, X., Wang, H., and Lu, K.: Interpretation of NO3-N2O5 observation via steady
516   state in high-aerosol air mass: the impact of equilibrium coefficient in ambient
517   conditions, Atmospheric Chemistry and Physics, 22, 3525-3533, 10.5194/acp-
518   22-3525-2022, 2022.

519   Chen, X. R., Wang, H. C., Liu, Y. H., Su, R., Wang, H. L., Lou, S. R., and Lu, K. D.:
520   Spatial characteristics of the nighttime oxidation capacity in the Yangtze River
521   Delta, China, Atmospheric Environment, 208, 150-157,
522   10.1016/j.atmosenv.2019.04.012, 2019.

523   Chen, X. R., Wang, H. C., Lu, K. D., Li, C. M., Zhai, T. Y., Tan, Z. F., Ma, X. F.,
524   Yang, X. P., Liu, Y. H., Chen, S. Y., Dong, H. B., Li, X., Wu, Z. J., Hu, M.,
525   Zeng, L. M., and Zhang, Y. H.: Field Determination of Nitrate Formation
526   Pathway in Winter Beijing, Environmental Science & Technology, 54, 9243-
527   9253, 10.1021/acs.est.0c00972, 2020.

528   Elshorbany, Y. F., Steil, B., Brühl, C., and Lelieveld, J.: Impact of HONO on global
529   atmospheric chemistry calculated with an empirical parameterization in the
530   EMAC model, ACP, 12, 9977-10000, 10.5194/acp-12-9977-2012, 2012.

531   Fountoukis, C. and Nenes, A.: ISORROPIA II: a computationally efficient
532   thermodynamic equilibrium model for K+-Ca2+-Mg2+-Nh(4)(+)-Na+-SO42--
533   NO3--Cl--H2O aerosols, Atmospheric Chemistry and Physics, 7, 4639-4659,
534   2007.

535   Goliff, W. S., Stockwell, W. R., and Lawson, C. V.: The regional atmospheric
536   chemistry mechanism, version 2, Atmospheric Environment, 68, 174-185,
537   10.1016/j.atmosenv.2012.11.038, 2013.

538 Guo, L., Hu, Y., Hu, Q., Lin, J., Li, C., Chen, J., Li, L., and Fu, H.: Characteristics
539   and chemical compositions of particulate matter collected at the selected metro
540   stations of Shanghai, China, Science of the Total Environment, 496, 443-452,
541   10.1016/j.scitotenv.2014.07.055, 2014.
542 Hagler, G. S. W., Bergin, M. H., Salmon, L. G., Yu, J. Z., Wan, E. C. H., Zheng, M.,
543   Zeng, L. M., Kiang, C. S., Zhang, Y. H., Lau, A. K. H., and Schauer, J. J.:
544   Source areas and chemical composition of fine particulate matter in the Pearl
545   River Delta region of China, Atmos. Environ., 40, 3802-3815,
546   10.1016/j.atmosenv.2006.02.032, 2006.
547 Jiang, M., Lu, K., Su, R., Tan, Z., Wang, H., Li, L., Fu, Q., Zhai, C., Tan, Q., Yue, D.,
548   Chen, D., Wang, Z., Xie, S., Zeng, L., and Zhang, Y.: Ozone formation and key
549   VOCs in typical Chinese city clusters, Chinese Sci Bull, 63, 1130-1141, 2018.
550 Kanaya, Y., Fukuda, M., Akimoto, H., Takegawa, N., Komazaki, Y., Yokouchi, Y.,
551   Koike, M., and Kondo, Y.: Urban photochemistry in central Tokyo: 2. Rates and
552   regimes of oxidant (O-3+NO2) production, Journal of Geophysical Research-
553   Atmospheres, 113, 10.1029/2007jd008671, 2008.
554 Li, H. Y., Zhang, Q., Zhang, Q., Chen, C. R., Wang, L. T., Wei, Z., Zhou, S.,
555   Parworth, C., Zheng, B., Canonaco, F., Prevot, A. S. H., Chen, P., Zhang, H. L.,
556   Wallington, T. J., and He, K. B.: Wintertime aerosol chemistry and haze
557   evolution in an extremely polluted city of the North China Plain: significant
558   contribution from coal and biomass combustion, Atmospheric Chemistry and
559   Physics, 17, 4751-4768, 2017.
560 Liu, X., Gu, J., Li, Y., Cheng, Y., Qu, Y., Han, T., Wang, J., Tian, H., Chen, J., and
561   Zhang, Y.: Increase of aerosol scattering by hygroscopic growth: Observation,
562   modeling, and implications on visibility, Atmos. Res., 132-133, 91-101,
563   https://doi.org/10.1016/j.atmosres.2013.04.007, 2013.
564 Lou, S., Tan, Z., Gan, G., Chen, J., Wang, H., Gao, Y., Huang, D., Huang, C., Li, X.,
565   Song, R., Wang, H., Wang, M., Wang, Q., Wu, Y., and Huang, C.: Observation
566   based study on atmospheric oxidation capacity in Shanghai during late-autumn:
567   Contribution from nitryl chloride, Atmospheric Environment, 271, 118902,
568   https://doi.org/10.1016/j.atmosenv.2021.118902, 2022.
569 Lu, K. D., Hofzumahaus, A., Holland, F., Bohn, B., Brauers, T., Fuchs, H., Hu, M.,
570   Haseler, R., Kita, K., Kondo, Y., Li, X., Lou, S. R., Oebel, A., Shao, M., Zeng,
571   L. M., Wahner, A., Zhu, T., Zhang, Y. H., and Rohrer, F.: Missing OH source in
572   a suburban environment near Beijing: observed and modelled OH and HO2
573   concentrations in summer 2006, Atmospheric Chemistry and Physics, 13, 1057-
574   1080, 10.5194/acp-13-1057-2013, 2013.
575 Lu, K. D., Rohrer, F., Holland, F., Fuchs, H., Bohn, B., Brauers, T., Chang, C. C.,
576   Haseler, R., Hu, M., Kita, K., Kondo, Y., Li, X., Lou, S. R., Nehr, S., Shao, M.,
577   Zeng, L. M., Wahner, A., Zhang, Y. H., and Hofzumahaus, A.: Observation and
578   modelling of OH and HO2 concentrations in the Pearl River Delta 2006: a
579   missing OH source in a VOC rich atmosphere, Atmospheric Chemistry and

580   Physics, 12, 1541-1569, 10.5194/acp-12-1541-2012, 2012.

581 Ma, X. F., Tan, Z. F., Lu, K. D., Yang, X. P., Chen, X. R., Wang, H. C., Chen, S. Y.,
582   Fang, X., Li, S. L., Li, X., Liu, J. W., Liu, Y., Lou, S. R., Qiu, W. Y., Wang, H.
583   L., Zeng, L. M., and Zhang, Y. H.: OH and HO2 radical chemistry at a suburban
584   site during the EXPLORE-YRD campaign in 2018, Atmospheric Chemistry and
585   Physics, 22, 7005-7028, 2022.

586 Meng, Z. Y., Wu, L. Y., Xu, X. D., Xu, W. Y., Zhang, R. J., Jia, X. F., Liang, L. L.,
587   Miao, Y. C., Cheng, H. B., Xie, Y. L., He, J. J., and Zhong, J. T.: Changes in
588   ammonia and its effects on PM2.5 chemical property in three winter seasons in
589   Beijing, China, Science of the Total Environment, 749, 2020.

590 Ming, L., Jin, L., Li, J., Fu, P., Yang, W., Liu, D., Zhang, G., Wang, Z., and Li, X.:
591   PM2.5 in the Yangtze River Delta, China: Chemical compositions, seasonal
592   variations, and regional pollution events, Environmental Pollution, 223, 200-212,
593   10.1016/j.envpol.2017.01.013, 2017.

594 Phillips, G. J., Thieser, J., Tang, M. J., Sobanski, N., Schuster, G., Fachinger, J.,
595   Drewnick, F., Borrmann, S., Bingemer, H., Lelieveld, J., and Crowley, J. N.:
596   Estimating N2O5 uptake coefficients using ambient measurements of NO3,
597   N2O5, ClNO2 and particle-phase nitrate, Atmospheric Chemistry and Physics,
598   16, 13231-13249, 10.5194/acp-16-13231-2016, 2016.

599 Qin, Y., Li, J. Y., Gong, K. J., Wu, Z. J., Chen, M. D., Qin, M. M., Huang, L., and
600   Hu, J. L.: Double high pollution events in the Yangtze River Delta from 2015 to
601   2019: Characteristics, trends, and meteorological situations, Science of the Total
602   Environment, 792, 10.1016/j.scitotenv.2021.148349, 2021.

603 Qiu, X. H., Ying, Q., Wang, S. X., Duan, L., Zhao, J., Xing, J., Ding, D., Sun, Y. L.,
604   Liu, B. X., Shi, A. J., Yan, X., Xu, Q. C., and Hao, J. M.: Modeling the impact of
605   heterogeneous reactions of chlorine on summertime nitrate formation in Beijing,
606   China, Atmospheric Chemistry and Physics, 19, 6737-6747, 10.5194/acp-19-
607   6737-2019, 2019.

608 Seinfeld, J. H. and Pandis, S. N.: Atmospheric chemistry and physics: from air
609   pollution to climate change, Third;3rd;,   Book, Whole, Wiley, Hoboken, New
610   Jersey2016.

611 Shang, D. J., Peng, J. F., Guo, S., Wu, Z. J., and Hu, M.: Secondary aerosol formation
612   in winter haze over the Beijing-Tianjin-Hebei Region, China, Front. Env. Sci.
613   Eng., 15, 13, 10.1007/s11783-020-1326-x, 2021.

614 Shu, L., Wang, T. J., Xie, M., Li, M. M., Zhao, M., Zhang, M., and Zhao, X. Y.:
615   Episode study of fine particle and ozone during the CAPUM-YRD over Yangtze
616   River Delta of China: Characteristics and source attribution, Atmospheric
617   Environment, 203, 87-101, 10.1016/j.atmosenv.2019.01.044, 2019.

618 Song, C. H. and Carmichael, G. R.: Gas-particle partitioning of nitric acid modulated
619   by alkaline aerosol, Journal of Atmospheric Chemistry, 40, 1-22, 2001.

620 Staudt, S., Gord, J. R., Karimova, N. V., McDuffie, E. E., Brown, S. S., Gerber, R. B.,
621   Nathanson, G. M., and Bertram, T. H.: Sulfate and Carboxylate Suppress the

622   Formation of ClNO2 at Atmospheric Interfaces, Acs Earth and Space Chemistry,
623   3, 1987-1997, 2019.
624 Sun, Y. L., Zhuang, G. S., Tang, A. H., Wang, Y., and An, Z. S.: Chemical
625   characteristics of PM2.5 and PM10 in haze-fog episodes in Beijing,
626   Environmental Science & Technology, 40, 3148-3155, 10.1021/es051533g,
627   2006.
628 Tan, Z., Wang, H., Lu, K., Dong, H., Liu, Y., Zeng, L., Hu, M., and Zhang, Y.: An
629   Observational Based Modeling of the Surface Layer Particulate Nitrate in the
630   North China Plain During Summertime, Journal of Geophysical Research:
631   Atmospheres, 126, e2021JD035623, https://doi.org/10.1029/2021JD035623,
632   2021.
633 Tan, Z. F., Lu, K. D., Dong, H. B., Hu, M., Li, X., Liu, Y. H., Lu, S. H., Shao, M., Su,
634   R., Wang, H. C., Wu, Y. S., Wahner, A., and Zhang, Y. H.: Explicit diagnosis of
635   the local ozone production rate and the ozone-NOx-VOC sensitivities, Science
636   Bulletin, 63, 1067-1076, 10.1016/j.scib.2018.07.001, 2018.
637 Tan, Z. F., Fuchs, H., Lu, K. D., Hofzumahaus, A., Bohn, B., Broch, S., Dong, H. B.,
638   Gomm, S., Haseler, R., He, L. Y., Holland, F., Li, X., Liu, Y., Lu, S. H., Rohrer,
639   F., Shao, M., Wang, B. L., Wang, M., Wu, Y. S., Zeng, L. M., Zhang, Y. S.,
640   Wahner, A., and Zhang, Y. H.: Radical chemistry at a rural site (Wangdu) in the
641   North China Plain: observation and model calculations of OH, HO2 and RO2
642   radicals, Atmospheric Chemistry and Physics, 17, 663-690, 10.5194/acp-17-663-
643   2017, 2017.
644 Tham, Y. J., Wang, Z., Li, Q., Wang, W., Wang, X., Lu, K., Ma, N., Yan, C.,
645   Kecorius, S., Wiedensohler, A., Zhang, Y., and Wang, T.: Heterogeneous N2O5
646   uptake coefficient and production yield of ClNO2 in polluted northern China:
647   roles of aerosol water content and chemical composition, Atmospheric
648   Chemistry and Physics, 18, 13155-13171, 10.5194/acp-18-13155-2018, 2018.
649 Wang, H., Zhu, B., Shen, L., Xu, H., An, J., Pan, C., Li, Y. e., and Liu, D.: Regional
650   Characteristics of Air Pollutants during Heavy Haze Events in the Yangtze River
651   Delta, China, Aerosol and Air Quality Research, 16, 2159-2171,
652   10.4209/aaqr.2015.09.0551, 2016.
653 Wang, H., Lu, K., Chen, X., Zhu, Q., Chen, Q., Guo, S., Jiang, M., Li, X., Shang, D.,
654   Tan, Z., Wu, Y., Wu, Z., Zou, Q., Zheng, Y., Zeng, L., Zhu, T., Hu, M., and
655   Zhang, Y.: High N2O5 Concentrations Observed in Urban Beijing: Implications
656   of a Large Nitrate Formation Pathway, Environmental Science and Technology
657   Letters, 4, 416-420, 10.1021/acs.estlett.7b00341, 2017a.
658 Wang, H. C. and Lu, K. D.: Determination and Parameterization of the Heterogeneous
659   Uptake Coefficient of Dinitrogen Pentoxide (N2O5), Prog. Chem., 28, 917-933,
660   10.7536/pc151225, 2016.
661 Wang, H. C., Chen, J., and Lu, K. D.: Development of a portable cavity-enhanced
662   absorption spectrometer for the measurement of ambient NO3 and N2O5:
663   experimental setup, lab characterizations, and field applications in a polluted

664   urban environment, Atmos. Meas. Tech., 10, 1465-1479, 10.5194/amt-10-1465-
665   2017, 2017b.
666 Wang, H. C., Lu, K. D., Chen, X. R., Zhu, Q. D., Wu, Z. J., Wu, Y. S., and Sun, K.:
667   Fast particulate nitrate formation via N2O5 uptake aloft in winter in Beijing,
668   Atmospheric Chemistry and Physics, 18, 10483-10495, 10.5194/acp-18-10483-
669   2018, 2018a.
670 Wang, H. C., Chen, X. R., Lu, K. D., Hu, R. Z., Li, Z. Y., Wang, H. L., Ma, X. F.,
671   Yang, X. P., Chen, S. Y., Dong, H. B., Liu, Y., Fang, X., Zeng, L. M., Hu, M.,
672   and Zhang, Y. H.: NO3 and N2O5 chemistry at a suburban site during the
673   EXPLORE-YRD campaign in 2018, Atmospheric Environment, 224, 9,
674   10.1016/j.atmosenv.2019.117180, 2020a.
675 Wang, H. C., Chen, X. R., Lu, K. D., Tan, Z. F., Ma, X. F., Wu, Z. J., Li, X., Liu, Y.
676   H., Shang, D. J., Wu, Y. S., Zeng, L. M., Hu, M., Schmitt, S., Kiendler-Scharr,
677   A., Wahner, A., and Zhang, Y. H.: Wintertime N2O5 uptake coefficients over
678   the North China Plain, Science Bulletin, 65, 765-774,
679   10.1016/j.scib.2020.02.006, 2020b.
680 Wang, H. C., Lu, K. D., Guo, S., Wu, Z. J., Shang, D. J., Tan, Z. F., Wang, Y. J., Le
681   Breton, M., Lou, S. R., Tang, M. J., Wu, Y. S., Zhu, W. F., Zheng, J., Zeng, L.
682   M., Hallquist, M., Hu, M., and Zhang, Y. H.: Efficient N2O5 uptake and NO3
683   oxidation in the outflow of urban Beijing, Atmospheric Chemistry and Physics,
684   18, 9705-9721, 10.5194/acp-18-9705-2018, 2018b.
685 Wang, S. B., Wang, L. L., Fan, X. G., Wang, N., Ma, S. L., and Zhang, R. Q.:
686   Formation pathway of secondary inorganic aerosol and its influencing factors in
687   Northern China: Comparison between urban and rural sites, Science of the Total
688   Environment, 840, 2022.
689 Wang, X. F., Zhang, Y. P., Chen, H., Yang, X., Chen, J. M., and Geng, F. H.:
690   Particulate Nitrate Formation in a Highly Polluted Urban Area: A Case Study by
691   Single-Particle Mass Spectrometry in Shanghai, Environmental Science &
692   Technology, 43, 3061-3066, 2009.
693 Wang, Z., Wang, W. H., Tham, Y. J., Li, Q. Y., Wang, H., Wen, L., Wang, X. F., and
694   Wang, T.: Fast heterogeneous N2O5 uptake and ClNO2 production in power
695   plant and industrial plumes observed in the nocturnal residual layer over the
696   North China Plain, Atmospheric Chemistry and Physics, 17, 12361-12378,
697   10.5194/acp-17-12361-2017, 2017c.
698 Woodward-Massey, R., Slater, E. J., Alen, J., Ingham, T., Cryer, D. R., Stimpson, L.
699   M., Ye, C. X., Seakins, P. W., Whalley, L. K., and Heard, D. E.: Implementation
700   of a chemical background method for atmospheric OH measurements by laser-
701   induced fluorescence: characterisation and observations from the UK and China,
702   Atmos. Meas. Tech., 13, 3119-3146, 10.5194/amt-13-3119-2020, 2020.
703 Wu, S. P., Dai, L. H., Zhu, H., Zhang, N., Yan, J. P., Schwab, J. J., and Yuan, C. S.:
704   The impact of sea-salt aerosols on particulate inorganic nitrogen deposition in
705   the western Taiwan Strait region, China, Atmos. Res., 228, 68-76, 2019.

706 Xia, M., Peng, X., Wang, W., Yu, C., Sun, P., Li, Y., Liu, Y., Xu, Z., Wang, Z., Xu,
707   Z., Nie, W., Ding, A., and Wang, T.: Significant production of ClNO2 and
708   possible source of Cl-2 from N2O5 uptake at a suburban site in eastern China,
709   Atmospheric Chemistry and Physics, 20, 6147-6158, 10.5194/acp-20-6147-2020,
710   2020.
711 Xu, J. W., Huang, X., Wang, N., Li, Y. Y., and Ding, A. J.: Understanding ozone
712   pollution in the Yangtze River Delta of eastern China from the perspective of
713   diurnal cycles, Science of the Total Environment, 752,
714   10.1016/j.scitotenv.2020.141928, 2021.
715 Xue, H., Liu, G., Zhang, H., Hu, R., and Wang, X.: Similarities and differences in
716   PM10 and PM2.5 concentrations, chemical compositions and sources in Hefei
717   City, China, Chemosphere, 220, 760-765, 10.1016/j.chemosphere.2018.12.123,
718   2019.
719 Yang, X. P., Lu, K. D., Ma, X. F., Liu, Y. H., Wang, H. C., Hu, R. Z., Li, X., Lou, S.
720   R., Chen, S. Y., Dong, H. B., Wang, F. Y., Wang, Y. H., Zhang, G. X., Li, S. L.,
721   Yang, S. D., Yang, Y. M., Kuang, C. L., Tan, Z. F., Chen, X. R., Qiu, P. P.,
722   Zeng, L. M., Xie, P. H., and Zhang, Y. H.: Observations and modeling of OH
723   and HO2 radicals in Chengdu, China in summer 2019, Science of the Total
724   Environment, 772, 2021.
725 Yu, C., Wang, Z., Xia, M., Fu, X., Wang, W. H., Tham, Y. J., Chen, T. S., Zheng, P.
726   G., Li, H. Y., Shan, Y., Wang, X. F., Xue, L. K., Zhou, Y., Yue, D. L., Ou, Y.
727   B., Gao, J., Lu, K. D., Brown, S. S., Zhang, Y. H., and Wang, T.: Heterogeneous
728   N2O5 reactions on atmospheric aerosols at four Chinese sites: improving model
729   representation of uptake parameters, Atmospheric Chemistry and Physics, 20,
730   4367-4378, 10.5194/acp-20-4367-2020, 2020a.
731 Yu, C. A., Wang, Z., Ma, Q. X., Xue, L. K., George, C., and Wang, T.: Measurement
732   of heterogeneous uptake of NO2 on inorganic particles, sea water and urban
733   grime, J. Environ. Sci., 106, 124-135, 10.1016/j.jes.2021.01.018, 2021.
734 Yu, D., Tan, Z., Lu, K., Ma, X., Li, X., Chen, S., Zhu, B., Lin, L., Li, Y., Qiu, P.,
735   Yang, X., Liu, Y., Wang, H., He, L., Huang, X., and Zhang, Y.: An explicit
736   study of local ozone budget and NOx-VOCs sensitivity in Shenzhen China,
737   Atmospheric Environment, 224, 117304, 10.1016/j.atmosenv.2020.117304,
738   2020b.
739 Zhang, K., Xu, J. L., Huang, Q., Zhou, L., Fu, Q. Y., Duan, Y. S., and Xiu, G. L.:
740   Precursors and potential sources of ground-level ozone in suburban Shanghai,
741   Front. Env. Sci. Eng., 14, 10.1007/s11783-020-1271-8, 2020a.
742 Zhang, R., Han, Y. H., Shi, A. J., Sun, X. S., Yan, X., Huang, Y. H., and Wang, Y.:
743   Characteristics of ambient ammonia and its effects on particulate ammonium in
744   winter of urban Beijing, China, Environ Sci Pollut R, 28, 62828-62838, 2021.
745 Zhang, Y., Hong, Z., Chen, J., Xu, L., Hong, Y., Li, M., Hao, H., Chen, Y., Qiu, Y.,
746   Wu, X., Li, J.-R., Tong, L., and Xiao, H.: Impact of control measures and
747   typhoon weather on characteristics and formation of PM2.5 during the 2016 G20

summit in China, Atmospheric Environment, 224, 117312,
https://doi.org/10.1016/j.atmosenv.2020.117312, 2020b.

Zhang, Y., Tang, L., Yu, H., Wang, Z., Sun, Y., Qin, W., Chen, W., Chen, C., Ding,
A., Wu, J., Ge, S., Chen, C., and Zhou, H.-c.: Chemical composition, sources and
evolution processes of aerosol at an urban site in Yangtze River Delta, China
during wintertime, Atmospheric Environment, 123, 339-349,
10.1016/j.atmosenv.2015.08.017, 2015.

Zhang, Y., Tang, L., Croteau, P. L., Favez, O., Sun, Y., Canagaratna, M. R., Wang,
Z., Couvidat, F., Albinet, A., Zhang, H., Sciare, J., Prevot, A. S. H., Jayne, J. T.,
and Worsnop, D. R.: Field characterization of the PM2.5 Aerosol Chemical
Speciation Monitor: insights into the composition, sources, and processes of fine
particles in eastern China, Atmospheric Chemistry and Physics, 17, 14501-
14517, 10.5194/acp-17-14501-2017, 2017.

Zhang, Y. Y., Tang, A. H., Wang, C., Ma, X., Li, Y. Z., Xu, W., Xia, X. P., Zheng, A.
H., Li, W. Q., Fang, Z. G., Zhao, X. F., Peng, X. L., Zhang, Y. P., Han, J.,
Zhang, L. J., Collett, J. L., and Liu, X. J.: PM (2.5) and water-soluble inorganic
ion concentrations decreased faster in urban than rural areas in China, J. Environ.
Sci., 122, 83-91, 2022.

Zhao, P. S., Dong, F., He, D., Zhao, X. J., Zhang, X. L., Zhang, W. Z., Yao, Q., and
Liu, H. Y.: Characteristics of concentrations and chemical compositions for
PM2.5 in the region of Beijing, Tianjin, and Hebei, China, Atmospheric
Chemistry and Physics, 13, 4631-4644, 10.5194/acp-13-4631-2013, 2013.

Zhao, Z. Z., Sun, N., Zhou, W. L., Ma, S. S., Li, X. D., Li, M. L., Zhang, X., Tang, S.
S., and Ye, Z. L.: Chemical Compositions in Winter PM2.5 in Changzhou of the
Yangtze River Delta Region, China: Characteristics and Atmospheric Responses
Along With the Different Pollution Levels, Front Env Sci-Switz, 10, 2022.

Zheng, G. J., Duan, F. K., Su, H., Ma, Y. L., Cheng, Y., Zheng, B., Zhang, Q., Huang,
T., Kimoto, T., Chang, D., Poschl, U., Cheng, Y. F., and He, K. B.: Exploring
the severe winter haze in Beijing: the impact of synoptic weather, regional
transport and heterogeneous reactions, Atmospheric Chemistry and Physics, 15,
2969-2983, 2015.